Fitoterapia 142 (2020) 104522

Contents lists available at ScienceDirect

Fitoterapia

journal homepage: www.elsevier.com/locate/fitote

Antidiabetic xanthones with α-glucosidase inhibitory activities from an endophytic *Penicillium canescens*

Abd. Malik[a,b], Hamidreza Ardalani[a], Syariful Anam[a,c], Laura Mikél McNair[a], Kresten J.K. Kromphardt[d], Rasmus John Normand Frandsen[d], Henrik Franzyk[a], Dan Staerk[a], Kenneth T. Kongstad[a,*]

[a] Department of Drug Design and Pharmacology, Faculty of Health and Medical Sciences, University of Copenhagen, Universitetsparken 2, DK-2100 Copenhagen, Denmark
[b] Faculty of Pharmacy, Universitas Muslim Indonesia, Jl. Urip Sumohardjo, Km. 5, 90231 Makassar, Indonesia
[c] Department of Pharmacy, Faculty of Mathematics and Sciences, Tadulako University, Palu, Indonesia
[d] Department of Biotechnology and Biomedicine, Technical University of Denmark, Søltofts Plads, Building 223, 2800 Kongens Lyngby, Denmark

ARTICLE INFO

Keywords:
Type 2 diabetes
Endophytic fungi
Penicillium canescens
α-Glucosidase inhibitors
Xanthone
Competitive inhibition

ABSTRACT

Worldwide, 463 million people are affected by diabetes of which the majority is diagnosed with Type 2 Diabetes (T2D). T2D can ultimately lead to retinopathy, nephropathy, nerve damage, and amputation of the lower extremities. α-Glucosidase, responsible for converting starch to monosaccharides, is a key therapeutic target for the management of T2D. However, due to substantial side effects of currently marketed drugs, there is an urgent need for the discovery of new α-glucosidase inhibitors. In our ongoing efforts to identify novel α-glucosidase inhibitors from Nature, we are investigating the potential of endophytic filamentous fungi as sustainable sources of hits and/or leads for future antihyperglycemic drugs. Here we report one previously unreported xanthone (**5**) and two known xanthones (**7** and **11**) as α-glucosidase inhibitors, isolated from an endophytic *Penicillium canescens*, recovered from fruits of *Juniperus polycarpos*. The three xanthones **5**, **7**, and **11** showed inhibitory activities against α-glucosidase with IC_{50} values of 38.80 ± 1.01 μM, 32.32 ± 1.01 μM, and 75.20 ± 1.02 μM, respectively. Further pharmacological characterization revealed a mixed-mode inhibition for **5**, a competitive inhibition for **7**, while **11** acted as a non-competitive inhibitor.

1. Introduction

At present, 463 million people are diagnosed with diabetes Worldwide, with 90% of the cases attributed to Type 2 diabetes (T2D). T2D is associated with fluctuations in the blood glucose levels, which can lead to several serious complications, including cardiovascular diseases, retinopathy, nephropathy, neuropathy, and amputation of lower extremities [1,2]. Moreover, T2D constitutes a severe economic societal burden, estimated to amount to USD 760 billion in annual global health expenditure in 2017 [2].

Due to its role in the enzymatic hydrolysis of starch-containing nutrients and certain disaccharides into glucose, inhibition of α-glucosidase constitutes a promising strategy for managing T2D [3,4]. Only a few α-glucosidase inhibitors (e.g., acarbose, miglitol, and voglibose) have been marketed, and these are all carbohydrate mimics and associated with multiple gastrointestinal adverse effects [4]. Thus, discovery of new non-carbohydrate drug leads targeting α-glucosidase might provide an approach for T2D treatment with less adverse effects, ultimately improving patient welfare.

Nature has proven to be a promising source of α-glucosidase inhibitors, e.g., compounds isolated from medicinal plants [5–9] and functional foods [9–13]. A complementary approach for discovering novel compounds, capable of inhibiting α-glucosidase, is to investigate the endophytic fungi associated with traditional medicinal plants.

Endophytic fungi are microorganisms living inside plant tissues in a non-pathogenic fashion. Here, fungi can produce secondary metabolites similar to or derivatives of those produced by the host plant [8,14,15]. This is the case for the anticancer compound paclitaxel, which is produced by the endophytic fungus *Taxomyces andreanae* as well as by its host plant Pacific yew [15]. Endophytes have also been shown to produce compounds that complement the host plant's defense, such as the insecticidal nodulisporic acid A, produced by *Nodilusporium* sp. isolated from woody plant tissue [16].

Identification of pharmacologically active compounds from natural sources is challenging due to chemical complexity of crude extracts. Here, we perform microfractionation of the crude extract into 96-well

* Corresponding author.
E-mail address: kenneth.kongstad@sund.ku.dk (K.T. Kongstad).

https://doi.org/10.1016/j.fitote.2020.104522
Received 14 January 2020; Received in revised form 17 February 2020; Accepted 19 February 2020
Available online 20 February 2020
0367-326X/

plates, used for creating a biochromatogram that can be used to pinpoint α-glucosidase inhibitory constituents directly from the crude extract. This technique has previously proved to be a very efficient methodology for identification of natural product-derived α-glucosidase inhibitors [6,12,13,17,18].

The genus *Juniperus* (Cupressaceae) has been used as antidiabetic traditional medicine on several continents [19,20], and hence it is an interesting as a potential source of antidiabetic endophyte-derived natural products. As part of our ongoing research on identification of potential T2D drug leads from endophytic filamentous fungi, we here report the structure elucidation and pharmacological characterization of α-glucosidase inhibitors from *Penicilliumcanescens* isolated from *Juniperuspolycarpos*. *P. canescens* has been reported to produce several antibiotic and antifungal secondary metabolites including canescin, griseofulvin, and various xanthones [21–24]. In this work, we report the α-glucosidase inhibitory effects of one (**5**) previously undescribed and two known xanthones from this fungal species.

2. Experimental section

2.1. Chemicals

α-Glucosidase from *Saccharomyces cerevisiae* type I, lyophilized powder (EC 3.2.1.20), *p*-nitrophenyl α-D-glucopyranoside (*p*-NPG), acarbose, sodium phosphate dehydrate, and disodium phosphate, sodium azide, $MgCl_2$, yeast extract peptone dextrose (YPD) medium, trisaminomethane (tris)/HCl, KCl, $(NH_4)_2SO_4$, $MgSO_4$, BSA and Triton-X were purchased from Sigma-Aldrich (Darmstadt, Germany); deoxynucleotide triphosphates (dNTPs) were purchased from Bio Basic (Markham, Canada), while dimethyl sulfoxide (DMSO) was purchased from Carl Roth (Karlsruhe, Germany). All primers were synthesized by TAG Copenhagen (Copenhagen, Denmark). Ethyl acetate, HPLC grade acetonitrile and methanol were obtained from VWR International (Fontenay-sous-Bois, France), while DMSO-d_6, chloroform-*d*, and methanol-d_4 were purchased from Eurisotop (Gif-Sur-Yvette Cedex, France). Formic acid, Potato Dextrose Agar (PDA), Yeast Extract Sucrose Agar (YES), and silica gel 60, 0.04–0.06 mm, were purchased from Merck (Darmstadt, Germany). Water was purified by 0.22 μM membrane filtration and deionized by using a Barnstead Nanopure system from Thermo Scientific (Waltham, MA, USA) or a Milli-Q Plus system (Millipore, Billerica, MA, USA). DNeasy UltraClean Microbil kit was purchased from Qiagen (Hilden, Germany), while GFX PCR DNA and Gel Band Purification kits were purchased from GE Healthcare (Chicago, IL, USA).

2.2. Isolation and identification of the fungal strain

Fruits of *Juniperus polycarpos* K. Koch var. *seravschanica* (Kom.) Kitam. were collected in Estahban, Iran (29.08°N, 54.04°E), placed in sealable bags, and stored at 4 °C until further use. No later than 48 h after collection, the fruits were cut into 5 mm pieces before being thoroughly washed in distilled water, and then submerged in 70% ethanol for 1 min, and then in 5% sodium hypochlorite for 2 min, after which they were thoroughly rinsed in sterile water three times. The surface-sterilized fruits were placed on PDA media in Petri dishes, and then incubated at 25 °C for 12 days. From these cultures, *P. canescens* was isolated and further cultivated on PDA. Identification of the new isolate was based on observations of the material's macro- and micro morphological features using a dichotomous identification key [25]. The morphology-based identification was subsequently supported by molecular genetic identification, using amplicon-sequencing of key genes. To generate sufficient biomass for DNA extraction, the strains were grown in liquid YPD medium for 8 days in darkness, at 25 °C with 150 rpm horizontal shaking. The biomass was filtered from the medium by using a piece of Miracloth, and washed with sterile MilliQ water. Genomic DNA was extracted using the DNeasy UltraClean Microbil kit following the manufacturers instructions. The ITS rDNA was PCR amplified with the ITS1 and ITS4 primers [26], and part of the *BenA* gene β-tubulin was amplified using the primers Bt2a and Bt2b [27]. Each 50 μL reaction mixture included 1 U *PfuX*7 DNA polymerase [28], CXL buffer (20 mM Tris/HCl, 10 mM KCl, 6 mM $(NH_4)_2SO_4$, 2 mM $MgSO_4$, 0.1 mg/mL BSA and 0.1% Triton-X [28], 0.4 μM of each primer, 200 μM dNTPs, 3% *v*/v DMSO, 3% v/v $MgCl_2$, ca. 10 ng gDNA and MilliQ water to 50 μL. The PCR reaction consisted of 98 °C for 3 min followed by 15 cycles of 98 °C for 30 s, touchdown annealing of 60–45 °C (−1 °C/cycle) for 30 s for ITS reactions and 65–50 °C (−1 °C/cycle) for 30 s for β-tubulin reactions, 72 °C for 1 min. These 15 cycles were followed by 20 cycles of 98 °C for 30 s, annealing at 53 °C for 30 s for ITS reactions and 63 °C for 30 s for β-tubulin reactions, 72 °C for 1 min. After the second round of cycles, a final elongation of 3 min at 72 °C was performed. The resulting DNA fragments were purified using the illustra GFX PCR DNA and Gel Band Purification Kit, and then Sanger sequenced by Eurofins genomics sequencing GmbH (Köln, Germany). The ITS fragments were sequenced using the ITS1 and ITS4 primers, while β-tubulin fragments were sequenced using the Bt2a and Bt2b primers. The obtained sequences were trimmed and assembled to consensus sequences using CLC Main Workbench (Qiagen, Hilden, Germany). The resulting consensus sequences were used for BLAST-n searches (NCBI, Bethesda, MD, USA) against the GeneBank NR database. The fungal isolate was a given a numerical identification number (ILF-002) and deposited in the Department of Drug Design and Pharmacology fungal collection kept in a − 80 °C temperature-surveyed freezer at University of Copenhagen.

2.3. Cultivation and extraction of P. canescens

P. canescens was three-point inoculated on 245 Petri dishes containing YES media, and then incubated at 27 °C for seven days. The fungal biomass and surrounding media were cut into approximately 1 × 1 cm pieces and extracted with ethyl acetate (6.5 L) by sonication for 1 h, and then the mixture was left at room temperature overnight to complete the extraction process. The extract was filtered through filter paper (AGF 118–145 mm, Frisenette, Knebel, Denmark), concentrated in vacuo, and then freeze-dried to yield crude ethyl acetate extract (6.7 g).

2.4. α-Glucosidase inhibition assay

The α-glucosidase inhibition assay was applied to both the crude fungal extract and pure compounds according to the protocol described by Schmidt and co-workers [29] with slight modifications. Briefly, the assays were performed in 96-well microplates using a Thermo Scientific Multiskan FC microplate photometer controlled by SkanIt version 2.5.1 software (Thermo Scientific, Waltham, MA, USA) with final volumes of 200 μL in each well. A 100 mM phosphate buffer was prepared by dissolving 2.65 g sodium hydrogen phosphate dehydrate, 4.70 g disodium phosphate, and 0.10 g sodium azide in 500 mL milli-Q water to produce a phosphate buffer containing 0.02% NaN_3 at pH 7.5. To each well, 10 μL of DMSO stock solution (2 mg/mL crude extract or 4 mM pure compound) was added, followed by 90 μL of 100 mM phosphate buffer (containing 0.02% NaN_3), and 80 μL α-glucosidase (2.0 U/mL in 100 mM phosphate buffer; enzyme solution). After shaking for 2 min, the microtiter plate was incubated at 28 °C for 10 min. Then, 20 μL of 10 mM *p*-NPG (substrate solution) was added to each well to initiate the reaction. The enzyme activity was determined by measuring the absorbance at 405 nm, representing the enzyme reaction product *p*-nitrophenol, every 30 s for 35 min.

2.5. HPLC separation and α-glucosidase inhibition profiling

Chromatographic separation was performed by using an Agilent 1200 series HPLC (Agilent 1200 series, Santa Clara, CA, USA),

consisting of a G1311A quaternary pump, a G1322A degasser, a G1316A thermostatted column compartment, a G1315C photodiode-array detector, a G1367C high-performance auto-sampler, and a G1364C fraction collector, all controlled by Agilent ChemStation ver. B.03.02 software and equipped with a reversed-phase Luna C18(2) column (Phenomenex, 150 × 4.6 mm, 3 μm particle size, 100 Å pore size, Torrance, CA, USA) maintained at 40 °C. The solvents used were: A (water: acetonitrile 95:5, *v*/v) and B (water: acetonitrile 5:95, v/v); both acidified with 0.1% (*v*/v) formic acid. The flow rate was maintained at 0.5 mL/min with the following gradient elution profile: 0 min, 20% B; 5 min, 40% B; 22 min, 40% B; 25 min, 100% B; 33 min, 100% B; 35 min, 20% B; and 40 min, 20% B. Twenty microliter crude extract (20 mg/mL in methanol) was injected, and the eluate was microfractionated from 5 to 40 min into 88 wells of a single 96-well microtiter plate.

The high-resolution biochromatogram of the prepurified fraction, containing compounds **4** and **5**, was obtained by using the HPLC system described above, equipped with a Phenomenex Kinetex pentafluorophenyl (PFP) column (150 × 4.60 mm, 2.6 μm particle size, 100 Å pore size, Torrance, CA, USA) maintained at 40 °C, and eluting it with a solvent system consisting of 95:5 water: methanol (*v*/v) (solvent A) and 5:95 water: methanol (v/v) (solvent B), both containing 0.1% (v/v) formic acid. Maintaining a solvent flow of 0.5 mL/min, the following gradient elution was used: 0 min, 40% B; 30 min, 100% B; 35 min, 100% B; 37 min, 40% B; and 42 min, 40% B. Ten μL of the fraction (10 mg/mL) was injected and microfractionated into 88 wells from 5 min to 40 min (2.51 data points per min).

The microplates were subsequently evaporated to dryness using a SPD121P Savant SpeedVac concentrator equipped with an RVT400 Refrigerated Vapor Trap and an OFP400 oil-free pump (ThermoFisher Scientific, Waltham, USA). The α-glucosidase inhibitory activity of the isolate in each well was determined by using the same instrument and method as previously described. The inhibitory activity expressed as percentage inhibition in each well was plotted below the HPLC-UV chromatogram, generating a biochromatogram.

2.6. Isolation of fungal metabolites

Fungal metabolites were isolated directly from the crude extract using a Shimadzu HPLC (Holm & Halby, Brøndby, Denmark) comprising a SPD-M20A prominence diode array detector, a LC-20AB binary pump, and a CTO-10A VP column oven, all controlled by Shimadzu LCsolution ver. 1.24 SP1, and equipped with a semi-preparative Phenomenex Luna C_{18}(2) HPLC column (250 × 10 mm, 5 μm particle size, 100 Å pore size, Torrance, CA, USA) kept at 40 °C. Separation using a mixture of solvent A (water:acetonitrile 95:5, *v*/v) and solvent B (water:acetonitrile 5:95, v/v), both acidified with 0.1% (*v*/v) formic acid, was performed according to the following gradient: 0 min, 20% B; 5 min, 40% B; 22 min, 40% B; 25 min, 100% B; 33 min, 100% B; 35 min, 20% B; and 40 min, 20% B at a flow rate of 4 mL/min. Twenty five sequential injections of 100 μL (100 mg/mL in methanol) yielded compounds **1** (4.76 mg, 1.9%), **2** (4.7 mg, 1.88%), **3** (0.31 mg, 0.12%), **4** (0.28 mg, 0.11%), **5** (0.16 mg, 0.06%), **6** (0.81 mg, 0.3%), **7** (0.74 mg, 0.29%), **8** (0.82 mg, 0.32%), **9** (0.69 mg, 0.28%), **10** (3.74 mg, 1.49%), **11** (1.06 mg, 0.42%), and **12** (2.59 mg, 1.04%).

2.7. Targeted isolation of compounds 4 and 5

For isolation of additional amounts of compounds **4** and **5**, crude ethyl acetate extract (3.0 g) was fractionated by means of vacuum liquid chromatography (11 × 10 cm i.d., column, 300 g of silica gel 60, 0.015–0.040 mm) and eluted with 5 × 100 mL ethyl acetat:methanol in the following step gradient 80:20; 60:40; 40:60; 20:80 0:100 (*v*/v) yielding fractions A-E 622 mg; 426 mg; 626 mg; 471 mg and 318 mg respectively. Fraction A, containing **4** and **5**, was separated using the semi-preparative column described in Section 2.6. In short, fraction A was dissolved in methanol (100 mg/mL in methanol) and injected 55 times (100 μL/injection) yielding 11.6 mg of a mixture enriched in **4** and **5**. This subfraction was further separated on a Phenomenex PFP column using the method described for the biochromatogram profile in Section 2.5, yielding **4** (2.27 mg, 0.41%) and **5** (0.78 mg, 0.14%).

2.8. HPLC-HRMS experiments

Mass spectra were acquired on an Agilent 1260 Series chromatographic HPLC system equipped with a G1329B autosampler, a G1311B quarternary pump with build-in degasser, a thermostated column compartment G1316A, equipped with reversed-phase column Luna C18(2) (Phenomenex, 150 × 4.6 mm, 3 μm particle size, 100 Å pore size, Inc., Torrance, CA, USA) maintained at 40 °C, and a G1315D photodiode-array detector. The HPLC was connected to a Bruker Daltoniks micrOTOF-QII mass spectrometer (Bruker Daltoniks, Bremen, Germany) equipped with an electrospray ionization (ESI) source. Mass spectra were acquired in negative-ion mode with a capillary voltage of 3500 V and in positive mode at 4100 V, a drying temperature of 200 °C, a nebulizer pressure of 2.0 bar, and a drying gas flow of 7 L/min. A solution of sodium formate was automatically injected at the beginning of the analysis to enable internal mass calibration. Chromatographic separation was performed by using the same method as described in Section 2.5.

2.9. NMR analysis

NMR spectra were acquired on a NMR instrument Bruker Avance III 600 MHz (operational frequency of 600.13 MHz) equipped with a 1.7-mm cryogenically cooled TCI probe and a Bruker SampleJet; samples were dissolved in methanol-d_4 (for compound **1**–**4** and **6**–**10**), DMSO-d_6 (for compound **5**) or in chloroform-*d* (for compound **11** and **12**). The spectra were acquired in automation (temperature equilibration to 300 K, optimization of lock parameters, gradient shimming, and setting of receiver gain). Automation of sample change and acquisition were controlled by IconNMR ver. 4.2 (Bruker Biopsin, Karlsruhe, Germany). Chemical shifts of ^{1}H and ^{13}C NMR data were referenced to the residual solvent signal (δ_H 3.31 ppm and δ_C 49.00 ppm for methanol-d_4, δ_H 2.50 ppm and δ_C 39.52 ppm for DMSO-d_6, and δ_H 7.26 ppm and δ_C 77.16 ppm for chloroform-*d*). ^{1}H spectra were acquired using 30° pulses, a spectral width of 20 ppm, acquisition time of 2.72 s, relaxation delay of 1.0 s, and collecting 64 k data points. DQF-COSY and NOESY spectra were acquired using a gradient-based pulse sequence with a spectral width of 12 ppm and collecting 2 k × 512 data points (processed with forward linear prediction to 2 k × 1 k data points). HSQC spectra were acquired with a spectral width of 12 ppm for ^{1}H and 170 ppm for ^{13}C, collecting 2 k × 256 data points (processed with forward linear prediction to 2 k × 1 k data points), and employing a relaxation delay of 1.0 s. HMBC spectra were acquired with a spectral width of 12 ppm for ^{1}H and 240 ppm for ^{13}C, collecting 2 k × 512 data points (processed with forward linear prediction to 2 k × 1 k data points), and using a relaxation delay of 1.0 s. Icon NMR (version 4.2, Bruker Biospin, Karlsruhe, Germany) was used for controlling the automated acquisition of NMR data, which was subsequently processed using Topspin (version 4.0.6, Bruker Biospin).

2.10. Determination of mode of inhibition

Measurements of enzyme kinetics of all active compounds were performed in triplicate according to Liu, et al. [11]. The experiments were performed based on the standard assay conditions as described in Section 2.4. In short, the mode of inhibition was determined by using a series of five *p*-NPG substrate concentrations (0.18, 0.37, 0.75, 1.5, and 3.0 mM) in the absence and presence of the active compounds (three concentrations). The reaction process was followed colorimetrically by measuring the absorbance at 405 nm every 30 s for 35 min.

2.11. Data analysis and interpretation

The inhibitory activity of the crude extract or pure compounds was calculated by using the following equation:

$$\text{Percent inhibition} = \frac{Slope(control) - Slope(sample)}{Slope(control)} \times 100\%$$

IC_{50} values were calculated by nonlinear regression curve fitting of the dose-response data (log concentration vs. percentage of inhibition).

$$f(x) = min + \frac{max - min}{1 + \left(\frac{x}{IC_{50}}\right)^{slope}}$$

where x is the concentration of the test compound, slope is the Hill slope, and min and max are the minimum and maximum concentrations for the sigmoidal curve. Data displayed in figures are presented as mean ± standard deviation (SD) for technical triplicates with an indication of *n*-values in the corresponding legend.

The kinetic parameters were calculated by using the Michaelis-Menten equation by fitting the kinetic rates to the substrate concentrations using nonlinear analysis [11]. Furthermore, the mode of inhibition was determined graphically from Lineweaver–Burk (double-reciprocal) plots of velocity against the substrate concentrations according to a rearranged Michaelis-Menten equation [11].

The IC_{50} values and kinetic calculations were performed using GraphPad Prism version 7.00 for Windows (GraphPad Software, La Jolla, California, USA).

3. Results and discussion

As part of our screening efforts to identify new α-glucosidase inhibitors, we investigated an endophytic filamentous fungi isolated from fruits of *Juniperus polycarpos* K. Koch var. *seravschanica* (Kom.) Kitam, because many *Juniperus* species have been used as traditional medicine for treatment of diabetes in e.g. Europe, Turkey, Algeria, Jordan, and Iran [20]. The species of the endophytic fungus investigated was determined by molecular genetic analysis of the Internal Transcribed Spacer (ITS) and β-tubulin (TUB) genes to be *Penicillium canescens* Sopp. The ITS and TUB sequences are provided in Supplementary Data Table S1 and also deposited in GenBank under accession number MN826829 and MN846268, respectively. The isolated fungus was cultivated on yeast extract succrose agar, extracted with ethyl acetate, and tested for the bioactivity at a concentration of 100 µg/mL, showing 99% inhibition of α-glucosidase as compared to the DMSO control. A dose-response curve was constructed based on a dilution series of the crude extract, revealing an IC_{50} value for α-glucosidase inhibition of 13.65 ± 0.13 µg/mL (Supplementary Data Fig. S1).

3.1. High-resolution α-glucosidase inhibition profiling

The active fungal metabolites, responsible for the observed α-glucosidase inhibitory activity, were pinpointed directly from the crude extract through microfractionation into 88 wells of a single 96-well microplate. The inhibitory activity of each well was plotted against the HPLC chromatograms at their respective retention times, yielding a biochromatogram with a resolution of 2.51 data points per min (Fig. 1). The biochromatogram indicated that compounds **4**/**5**, **7**, and **12** were

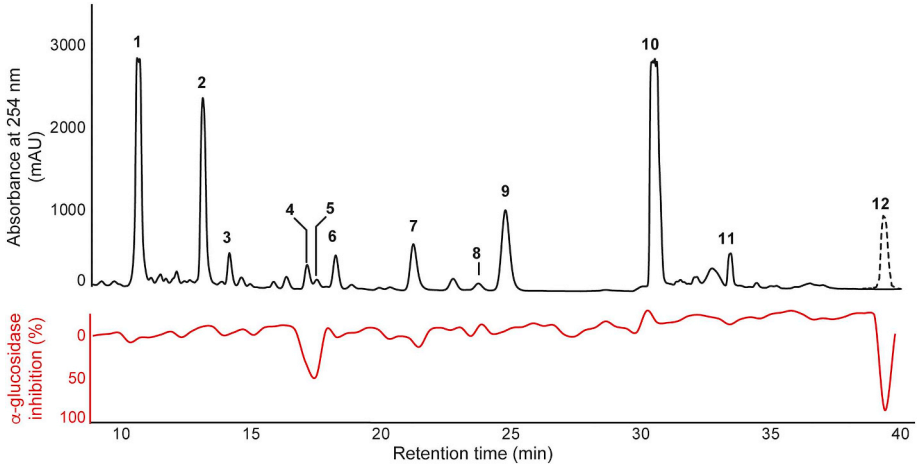

Fig. 1. HPLC chromatogram of the crude fungal ethyl acetate extract separated on a C_{18} column and monitored at 254 nm (black) with 210 nm inserted for compound **12** (dashed grey). The corresponding high-resolution α-glucosidase inhibition profile (red) is shown below. (For interpretation of the references to colour in this figure legend, the reader is referred to the web version of this article.)

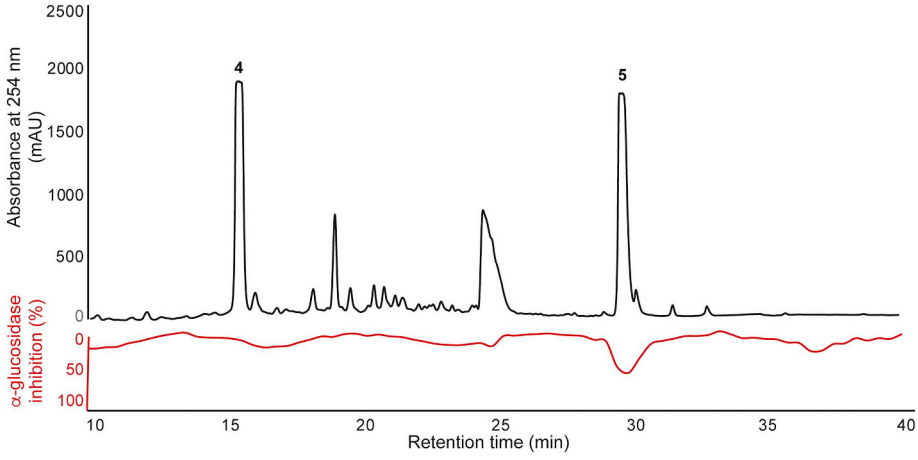

Fig. 2. HPLC chromatogram of pre-purified fungal ethyl acetate extract, containing compound **4** and **5**, separated on a PFP column and monitored at 254 nm (black) with the corresponding high-resolution α-glucosidase inhibition profile shown below (red). (For interpretation of the references to colour in this figure legend, the reader is referred to the web version of this article.)

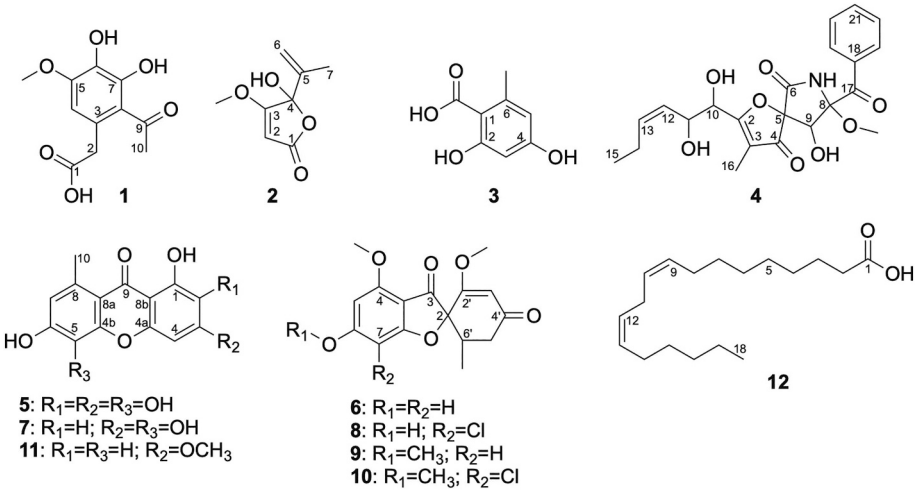

Fig. 3. Structures of **1–12** isolated from *P. canescens*.

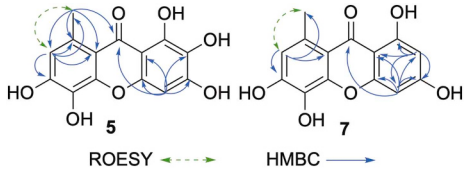

Fig. 4. Key ROESY and HMBC correlations for **5** and **7**.

inhibitors of α-glucosidase, as the inhibition correlating with these peaks was above 20%. As compounds **4** and **5** were not adequately separated on the C_{18} column, these were isolated as a mixture and subsequently microfractionated using a PFP column (Fig. 2), identifying compound **5** as being active while **4** was inactive.

3.2. Identification of metabolites

From the ethyl acetate extract of the endophytic fungus *P. canescens,* one previously undescribed xanthone (**5**), and 11 known compounds, were isolated and identified (Fig. 3). The structures of known compounds were determined by comparing their HR-ESIMS, UV–Vis, and NMR data with those previously reported (see Supplementary Data Table S2) to be vulculic acid (**1**) [30], penicillic acid (**2**) [31], orsellinic acid (**3**) [32], pseurotin A (**4**) [33], 1,3,5,6-tetrahydroxy-8-methylxanthone (**7**) [34], 1,6-dihydroxy-3-methoxy-8-methylxanthone (**11**) [35], griseofulvin (**10**) [36] and three related compounds: 6-desmethyl-dechlorogriseofulvin (**6**) [36], 6-desmethyl-griseofulvin (**8**) [36], and dechlorogriseofulvin (**9**) [36] as well as the fatty acid linoleic acid (**12**) [11]. Of these, this is the first report of **1**, **5, 6, 8**, and **12** isolated from *P. canescens.* Retention time, UV absorbance, HRMS and ^{1}H NMR data of all compounds are provided in Supplementary Data Table S2, and MS spectra of **8** and **10** are provided in Supplementary Data Fig. S2, with an isotope pattern supporting the presence of one chlorine atom in both **8** and **10**.

Table 1
^{1}H NMR (600 MHz), ^{13}C NMR (150 MHz) and HMBC spectral data of **5** in dimethylsulfoxide-d_6 (δ in ppm).

Position	δ_C, type[a]	δ_H (nH, multiplicity)	HMBC correlations[b]
2	125.6, C	–	–
3	155.8, C	–	–
4	97.50, CH	6.04 (1H, s)	C-8b, C-2, C-4a, C-3, C-9[c]
4a	154.5, C	–	–
4b	129.7, C	–	–
5	136.2, C	–	–
6	152.1, C	–	–
7	115.4, CH	6.53 (1H, s)	C-8a, C-8, C-6, C-10
8	131.9, C	–	–
8a	110.0, C	–	–
8b	100.2, C	–	–
9	181.4, C=O	–	–
10	22.1, CH_3	2.61 (3H, s)	C-8a, C-7, C-4b, C-8, C-9[c]
1-OH		12.94 (OH, br s)	–
OH		8.47 (5 OH, br s)	–

[a] ^{13}C data were obtained from HMBC and HSQC spectra.
[b] Correlations from H in to the indicated C.
[c] long-range HMBC.

Compound **5** was obtained as a yellow powder, UV (MeOH) λ_{max} 222, 255, and 333 nm, with a pseudomolecular ion of *m/z* 289.0356 (corresponding to $C_{14}H_9O_7^-$, Δ 1.4 ppm) in HR-ESIMS(−). The molecular formula as well as the UV spectrum indicated that compound **5** was an oxygenated analog of 1,3,5,6-tetrahydroxy-8-methylxanthone (**7**). This was confirmed by inspection of the ^{1}H NMR spectrum that displayed two aromatic singlets at 6.53 ppm and 6.04 ppm, a broad hydrogen-bonded hydroxyl group, seen at 12.94 ppm (OH-1), and a methyl group at 2.61 ppm. A HMBC correlation from H-10 to C-7, C-8, C-8a, and C-9 allowed assignment of the methyl group to C-8, while a ROE correlation between H-10 and the singlet for H-7 at δ_H 6.53 as well as HMBC correlations from H-7 to C-6 (δ_C 152.1), C-8 and C-8a proved H-7 to be between the methyl group and a hydroxyl group. Observing H-7 as a singlet allowed assignment of hydroxyl groups to C-5 and C-6. With a HSQC correlation to a carbon at 97.5 ppm and strong ^3J HMBC correlations to carbons at 100.2 ppm and 125.6 ppm, the remaining aromatic singlet could potentially be assigned to either C-2 or C-4. In previous studies, HMBC correlations from the aromatic proton to C-1 have been used to assign position C-2 [37]. However, due to low solubility in chloroform-*d*, C-1 could not be unambigously assigned, and hence this was not a viable approach. Acquisition of a long-range HMBC spectrum (optimized for 3 Hz couplings) displayed correlations

Table 2
IC_{50} values of crude fungal extract and active compounds.

Compound	Extract/compound	IC_{50} values[a,b]
	Crude ethyl acetate extract	13.65 ± 0.13[c]
5	1,2,3,5,6-pentahydroxy-8-methylxanthone	38.80 ± 1.01
7	1,3,5,6-Tetrahydroxy-8-methylxanthone	32.32 ± 1.01
11	1,6-Dihydroxy-3-methoxy-8-methylxanthone	75.20 ± 1.02
12	Linoleic acid	62.69 ± 1.03
Reference	Acarbose	969.70 ± 6.62

[a] IC_{50} values given as mean value ± SD (n = 3).
[b] μM.
[c] μg/mL.

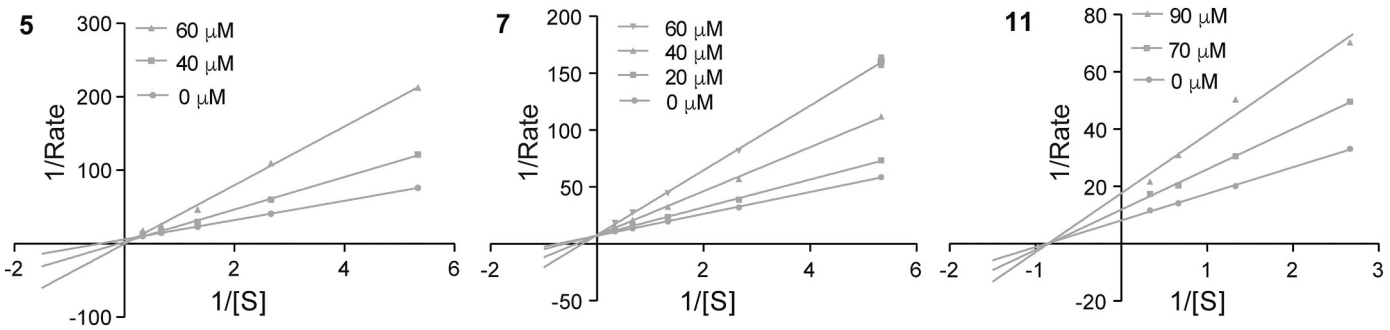

Fig. 5. Lineweaver-Burk plots to determine the mode of inhibition of **5**, **7**, and **11** against α-glucosidase. Each data point represents mean ± SD of three replicates (the SD values are in most cases very small, and hence covered by the mean data point and not visible in the graphs).

between the unassigned aromatic proton and the carbonyl (Fig. 4). While both the possible positions of the remaining aryl-H (C-2 or C-4) would result in ^{4}J couplings, comparison with the known analog, compound **7**, revealed that only the proton at C-4 gave give rise to the observed HMBC correlation. This allowed us to identify compound **5** as 1,2,3,5,6-pentahydroxy-8-methylxanthone. ^{1}H NMR, COSY, ROESY, HSQC and HMBC spectra of **5** is provided in Supplementary Data Fig. S3-S8, selected ROESY and HMBC correlations for **5** and **7** are shown in Fig. 4, while fully assigned ^{1}H and ^{13}C NMR data are provided in Table 1.

3.3. Pharmacological characterization of identified α-glucosidase inhibitors

The biochromatograms in Figs. 1 and 2 correlated **5, 7,** and **12** with α-glucosidase inhibitory activity. In contrast, compound **11**, which shows close structural similarity with **5** and **7**, was not correlated with α-glucosidase inhibitory activity; either due to a lower inhibitory activity or a lower abundance. Thus, dose-response curves were prepared from dilution series of **5**, **7**, **11**, and **12** (Supplementary Data Fig. S1), and IC_{50} values determined from these are shown in Table 2. With IC_{50} values of 38.8 and 33.2 μM for **5** and **7**, respectively, their α-glucosidase inhibitory activity is approxmately double as strong as **11**, showing an IC_{50} value of 75.2 μM. This, indicates that **11**'s missing correlation with inhibitory activity in Fig. 1 is mainly due to a lower inhibitory activity, because the crude extract contains 0.42% of **11** (not correlated with bioactivity in Figs. 1) and only 0.14% of **5** (correlated with bioactivity in Figs. 1 and 2). The IC_{50} values of **5**, **7** and **11** are in good agreement with IC_{50} values reported for related analogs [38–42]. Compound **12** showed an IC_{50} value of 62.69 μM in our study, which is in relative good agreement with another study, reporting linoleic acid (**12**) as an α-glucosidase inhibitor with an IC_{50} value of 75 μM, and with a mixed-mode inhibition [11].

Studies of the α-glucosidase-inhibitory activity of xanthones have shown that the activity primarily depends on the presence of hydroxyl groups, facilitating hydrogen bonding, but also the π-π stacking interactions of the xanthones has been shown to be important for the α-glucosidase inhibitory activities [38,40]. This explains the observed IC_{50} values for the highly hydroxylated **5** and **7** being more potent than the least hydroxylated **11**. Interestingly, the additional hydroxyl group in **5** (in position C-2) as compared to **7,** did not increase the observed activity. This indicates that the hydroxyl group at this position may not be involved in essential enzyme-ligand interactions. This is further corroborated by Liu and coworkers showing that the positioning of hydroxyl groups in xanthone derivatives is a determining factor for their α-glucosidase inhibitory activity, concluding that the inhibitory activity does not solely depend on the total number of hydroxyl groups [41].

Interestingly, even though compounds **5**, **7**, and **11** are structurally very similar, their Lineweaver-Burk plots [43] revealed different modes of inhibition (Fig. 5). Compound **7** proved to be a competitive inhibitor, having an interception point at the Y-axis, while compound **11**, with the interception positioned at the X-axis, was shown to be a non-competitive inhibitor. The Lineweaver-Burk plot of compound **5** had an interception point in the first quadrant (+X, +Y), which suggests a mixed-mode inhibition of α-glucosidase. This is a very unusual inhibition pattern, but this has previously been reported by Masson and coworkers when investigating benzalkonium as inhibitor of wild-type butyrylcholin esterase [44].

4. Conclusion

In the present study, the ethyl acetate extract of *P. canescens* cultivated on yeast extract sucrose agar was investigated for α-glucosidase-inhibitory constituents. α-Glucosidase inhibitory profiling, combined with semi-preparative and analytical-scale chromatographic separation led to isolation of three α-glucosidase inhibitory xanthones (**5**, **7**, and **11**), of which **5** is described for the first time. The mode of inhibition of α-glucosidase was investigated, showing **5** to be a mixed-mode inhibitor, **7** to be a competitive inhibitor, and **11** to be a non-competitive inhibitor. This work underlines the potential of endophytic filamentous fungi as a source of interesting natural products with inhibitory acitivity against yeast α-glucosidase. However, further studies of these compounds' inhibitory acitivity against mammalian α-glucosidase as well as assessment of their cytotoxicity are first steps needed before drawing any conclusions of their potential for management of type 2 diabetes.

Declaration of Competing Interest

The authors declare no conflict of interest.

Acknowledgments

The HPLC-HRMS and NMR equipment were acquired through a grant from “Apotekerfonden af 1991”, The Carlsberg Foundation, and the Danish Agency for Science, Technology, and Innovation via the National Research Infrastructure funds. Arife Önder and Katrine Juhl Krydsfeldt are acknowledged for their technical assistance. AM was supported by Lembaga Pengelola Dana Pendidikan (LPDP), Ministry of Finance, Republic of Indonesia, through the BUDI-LN scholarship program 2016. KJKK and RJNF was supported by The Danish National Research Foundation (DNRF137) for the Center for Microbial Secondary Metabolites.

Appendix A. Supplementary data

Supplementary data to this article can be found online at https://doi.org/10.1016/j.fitote.2020.104522.

References

[1] American Diabetes Association, Diagnosis and classification of diabetes mellitus, Diabetes Care 36 (Suppl. 1) (2013) S67–S74, https://doi.org/10.2337/dc13-S067.

[2] International Diabetes Federation, IDF Diabetes Atlas, 9th ed, (2019) Brussels, Belgium. Online version at http://www.diabetesatlas.org/ ((accessed December 16, 2019). ISBN: 978-2-930229-87-4).

[3] S. Chiba, Molecular mechanism in α-glucosidase and glucoamylase, Biosci. Biotechnol. Biochem. 61 (8) (1997) 1233–1239, https://doi.org/10.1271/bbb.61.1233.

[4] J. Upadhyay, S.A. Polyzos, N. Perakakis, B. Thakkar, S.A. Paschou, N. Katsiki, P. Underwood, K.H. Park, J. Seufert, E.S. Kang, E. Sternthal, A. Karagiannis, C.S. Mantzoros, Pharmacotherapy of type 2 diabetes: an update, Metabolism 78 (2018) 13–42, https://doi.org/10.1016/j.metabol.2017.08.010.

[5] B.T.D. Trinh, D. Staerk, A.K. Jager, Screening for potential α-glucosidase and α-amylase inhibitory constituents from selected Vietnamese plants used to treat type 2 diabetes, J. Ethnopharmacol. 186 (2016) 189–195, https://doi.org/10.1016/j.jep.2016.03.060.

[6] S.G. Wubshet, Y. Tahtah, A.M. Heskes, K.T. Kongstad, I. Pateraki, B. Hamberger, B.L. Moller, D. Staerk, Identification of PTP1B and α-glucosidase inhibitory serrulatanes from *Eremophila* spp. by combined use of dual high-resolution PTP1B and α-glucosidase inhibition profiling and HPLC-HRMS-SPE-NMR, J. Nat. Prod. 79 (4) (2016) 1063–1072, https://doi.org/10.1021/acs.jnatprod.5b01128.

[7] B. Liu, K.T. Kongstad, S. Qinglei, N.T. Nyberg, A.K. Jager, D. Staerk, Dual high-resolution α-glucosidase and radical scavenging profiling combined with HPLC-HRMS-SPE-NMR for identification of minor and major constituents directly from the crude extract of *Pueraria lobata*, J. Nat. Prod. 78 (2) (2015) 294–300, https://doi.org/10.1021/np5009416.

[8] G.A. Strobel, Endophytes as sources of bioactive products, Microbes Infect. 5 (6) (2003) 535–544, https://doi.org/10.1016/S1286-4579(03)00073-X.

[9] S. Wiese, S.G. Wubshet, J. Nielsen, D. Staerk, Coupling HPLC-SPE-NMR with a microplate-based high-resolution antioxidant assay for efficient analysis of antioxidants in food-validation and proof-of-concept study with caper buds, Food Chem. 141 (4) (2013) 4010–4018, https://doi.org/10.1016/j.foodchem.2013.06.115.

[10] S.G. Wubshet, J.S. Schmidt, S. Wiese, D. Staerk, High-resolution screening combined with HPLC-HRMS-SPE-NMR for identification of potential health-promoting constituents in sea aster and searocket-new Nordic food ingredients, J. Agric. Food Chem. 61 (36) (2013) 8616–8623, https://doi.org/10.1021/jf402949y.

[11] B. Liu, K.T. Kongstad, S. Wiese, A.K. Jager, D. Staerk, Edible seaweed as future functional food: identification of α-glucosidase inhibitors by combined use of high-resolution alpha-glucosidase inhibition profiling and HPLC-HRMS-SPE-NMR, Food Chem. 203 (2016) 16–22, https://doi.org/10.1016/j.foodchem.2016.02.001.

[12] Y. Zhao, M.X. Chen, K.T. Kongstad, A.K. Jager, D. Staerk, Potential of *Polygonum cuspidatum* root as an antidiabetic food: dual high-resolution α-glucosidase and PTP1B inhibition profiling combined with HPLC-HRMS and NMR for identification of antidiabetic constituents, J. Agric. Food Chem. 65 (22) (2017) 4421–4427, https://doi.org/10.1021/acs.jafc.7b01353.

[13] C. Liang, D. Staerk, K.T. Kongstad, Potential of *Myrtus communis* Linn. as a bi-functional food: Dual high-resolution PTP1B and α-glucosidase inhibition profiling combined with HPLC-HRMS and NMR for identification of antidiabetic triterpenoids and phloroglucinol derivatives, J. Funct. Foods (2019), https://doi.org/10.1016/j.jff.2019.103623 103623.

[14] S. Kusari, S.P. Pandey, M. Spiteller, Untapped mutualistic paradigms linking host plant and endophytic fungal production of similar bioactive secondary metabolites, Phytochemistry 91 (2013) 81–87, https://doi.org/10.1016/j.phytochem.2012.07.021.

[15] A. Stierle, G. Strobel, D. Stierle, Taxol and taxane production by *Taxomyces andreanae*, an endophytic fungus of Pacific yew, Science 260 (5105) (1993) 214–216, https://doi.org/10.1126/science.8097061.

[16] J.G. Ondeyka, G.L. Helms, O.D. Hensens, M.A. Goetz, D.L. Zink, A. Tsipouras, W.L. Shoop, L. Slayton, A.W. Dombrowski, J.D. Polishook, D.A. Ostlind, N.N. Tsou, R.G. Ball, S.B. Singh, Nodulisporic Acid A, a Novel and potent insecticide from a *Nodulisporium* Sp. isolation, structure determination, and chemical transformations, J. Am. Chem. Soc. 119 (38) (1997) 8809–8816, https://doi.org/10.1021/ja971664k.

[17] Y. Zhao, K.T. Kongstad, A.K. Jager, J. Nielsen, D. Staerk, Quadruple high-resolution α-glucosidase/α-amylase/PTP1B/radical scavenging profiling combined with high-performance liquid chromatography-high-resolution mass spectrometry-solid-phase extraction-nuclear magnetic resonance spectroscopy for identification of antidiabetic constituents in crude root bark of *Morus alba* L, J. Chromatogr. A 1556 (2018) 55–63, https://doi.org/10.1016/j.chroma.2018.04.041.

[18] K.T. Kongstad, C. Ozdemir, A. Barzak, S.G. Wubshet, D. Staerk, Combined use of high-resolution α-glucosidase inhibition profiling and high-performance liquid chromatography-high-resolution mass spectrometry-solid-phase extraction-nuclear magnetic resonance spectroscopy for investigation of antidiabetic principles in crude plant extracts, J. Agric. Food Chem. 63 (8) (2015) 2257–2263, https://doi.org/10.1021/jf506297k.

[19] N. Orhan, M. Aslan, B. Demirci, F. Ergun, A bioactivity guided study on the antidiabetic activity of *Juniperus oxycedrus subsp. oxycedrus* L. leaves, J. Ethnopharmacol. 140 (2) (2012) 409–415, https://doi.org/10.1016/j.jep.2012.01.042.

[20] N. Orhan, Juniperus Species: Features, profile and applications to diabetes, in: R.R. Watson, V.R. Preedy (Eds.), Bioactive Food as Dietary Interventions for Diabetes, Second ed., Academic Press, 2019, pp. 447–459, , https://doi.org/10.1016/B978-0-12-813822-9.00030-8 Chapter 30.

[21] M. Frank, R. Hartmann, M. Plenker, A. Mandi, T. Kurtan, F.C. Ozkaya, W.E.G. Muller, M.U. Kassack, A. Hamacher, W. Lin, Z. Liu, P. Proksch, Brominated azaphilones from the sponge-associated fungus *Penicillium canescens* strain 4.14.6a, J. Nat. Prod. 82 (8) (2019) 2159–2166, https://doi.org/10.1021/acs.jnatprod.9b00151.

[22] P.W. Brian, H.G. Hemming, J.S. Moffatt, C.H. Unwin, Canescin, an antibiotic produced by *Penicillium canescens*, Trans. Br. Mycol. Soc. 36 (3) (1953) 243–247, https://doi.org/10.1016/S0007-1536(53)80009-4.

[23] B.V. Bertinetti, N.I. Pena, G.M. Cabrera, An antifungal tetrapeptide from the culture of *Penicillium canescens*, Chem. Biodivers. 6 (8) (2009) 1178–1184, https://doi.org/10.1002/cbdv.200800336.

[24] R. Nicoletti, M.P. Lopez-Gresa, E. Manzo, A. Carella, M.L. Ciavatta, Production and fungitoxic activity of Sch 642305, a secondary metabolite of *Penicillium canescens*, Mycopathologia 163 (5) (2007) 295–301, https://doi.org/10.1007/s11046-007-9015-x.

[25] P.W. Crous, G.J.M. Verkley, J.Z. Groenewald, R.A. Samson, Fungal Biodiversity, 1 CBS Laboratory Manual Series, Utrecht, 2009 (ISBN: 9789070351779).

[26] T.J. White, T. Bruns, S. Lee, J. Taylor, Amplification and direct sequencing of fungal ribosomal RNA genes for phylogenetics, PCR Protocols 18 (1) (1990) 315–322, https://doi.org/10.1016/b978-0-12-372180-8.50042-1.

[27] N.L. Glass, G.C. Donaldson, Development of primer sets designed for use with the PCR to amplify conserved genes from filamentous ascomycetes, Appl. Environ. Microbiol. 61 (4) (1995) 1323–1330 (PMCID: PMC167388).

[28] M.H.H. Nørholm, A mutant Pfu DNA polymerase designed for advanced uracil-excision DNA engineering, BMC Biotechnol. 10 (1) (2010) 21, https://doi.org/10.1186/1472-6750-10-21.

[29] J.S. Schmidt, M.B. Lauridsen, L.O. Dragsted, J. Nielsen, D. Staerk, Development of a bioassay-coupled HPLC-SPE-ttNMR platform for identification of α-glucosidase inhibitors in apple peel (*Malus domestica* Borkh.), Food Chem. 135 (3) (2012) 1692–1699, https://doi.org/10.1016/j.foodchem.2012.05.075.

[30] Y. Kimura, M. Nishibe, H. Nakajima, T. Hamasaki, Vulculic acid, a pollen germination inhibitor produced by the fungus, *Penicillium* sp, Agric. Biol. Chem. 55 (4) (1991) 1137–1138, https://doi.org/10.1080/00021369.1991.10870695.

[31] T.T. Bladt, C. Durr, P.B. Knudsen, S. Kildgaard, J.C. Frisvad, C.H. Gotfredsen, M. Seiffert, T.O. Larsen, Bio-activity and dereplication-based discovery of ophiobolins and other fungal secondary metabolites targeting leukemia cells, Molecules 18 (12) (2013) 14629–14650, https://doi.org/10.3390/molecules181214629.

[32] J.F. Sanchez, Y.M. Chiang, E. Szewczyk, A.D. Davidson, M. Ahuja, C. Elizabeth Oakley, J. Woo Bok, N. Keller, B.R. Oakley, C.C. Wang, Molecular genetic analysis of the orsellinic acid/F9775 gene cluster of *Aspergillus nidulans*, Mol. BioSyst. 6 (3) (2010) 587–593, https://doi.org/10.1039/b904541d.

[33] G. Schmeda-Hirschmann, E. Hormazabal, J.A. Rodriguez, C. Theoduloz, Cycloaspeptide A and pseurotin A from the endophytic fungus *Penicillium janczewskii*, Z. Naturforsch. C. J. Biosci. 63 (5–6) (2008) 383–388, https://doi.org/10.1515/znc-2008-5-612.

[34] G.N. Belofsky, K.B. Gloer, J.B. Gloer, D.T. Wicklow, P.F. Dowd, New p-terphenyl and polyketide metabolites from the sclerotia of *Penicillium raistrickii*, J. Nat. Prod. 61 (9) (1998) 1115–1119, https://doi.org/10.1021/np980188o.

[35] J. Mutanyatta, B.G. Matapa, D.D. Shushu, B.M. Abegaz, Homoisoflavonoids and xanthones from the tubers of wild and in vitro regenerated *Ledebouria graminifolia* and cytotoxic activities of some of the homoisoflavonoids, Phytochemistry 62 (5) (2003) 797–804, https://doi.org/10.1016/s0031-9422(02)00622-2.

[36] N.D. Paguigan, M.H. Al-Huniti, H.A. Raja, A. Czarnecki, J.E. Burdette, M. Gonzalez-Medina, J.L. Medina-Franco, S.J. Polyak, C.J. Pearce, M.P. Croatt, N.H. Oberlies, Chemoselective fluorination and chemoinformatic analysis of griseofulvin: natural vs fluorinated fungal metabolites, Bioorg. Med. Chem. 25 (20) (2017) 5238–5246, https://doi.org/10.1016/j.bmc.2017.07.041.

[37] C. Abdel-Lateff, G.M. Klemke, A.D. Konig, Wright, two new xanthone derivatives from the algicolous marine fungus *Wardomyces anomalus*, J. Nat. Prod. 66 (5) (2003) 706–708, https://doi.org/10.1021/np020518b.

[38] Y. Liu, L. Ma, W.H. Chen, B. Wang, Z.L. Xu, Synthesis of xanthone derivatives with extended pi-systems as α-glucosidase inhibitors: insight into the probable binding mode, Bioorg. Med. Chem. 15 (8) (2007) 2810–2814, https://doi.org/10.1016/j.bmc.2007.02.030.

[39] C.M.M. Santos, M. Freitas, E. Fernandes, A comprehensive review on xanthone derivatives as α-glucosidase inhibitors, Eur. J. Med. Chem. 157 (2018) 1460–1479, https://doi.org/10.1016/j.ejmech.2018.07.073.

[40] Y. Liu, L. Ma, W.H. Chen, H. Park, Z. Ke, B. Wang, Binding mechanism and

synergetic effects of xanthone derivatives as noncompetitive α-glucosidase inhibitors: a theoretical and experimental study, J. Phys. Chem. B 117 (43) (2013) 13464–13471, https://doi.org/10.1021/jp4067235.
[41] Y. Liu, L. Zou, L. Ma, W.H. Chen, B. Wang, Z.L. Xu, Synthesis and pharmacological activities of xanthone derivatives as α-glucosidase inhibitors, Bioorg. Med. Chem. 14 (16) (2006) 5683–5690, https://doi.org/10.1016/j.bmc.2006.04.014.
[42] C. Uvarani, K. Arumugasamy, K. Chandraprakash, M. Sankaran, A. Ata, P.S. Mohan, A new DNA-intercalative cytotoxic allylic xanthone from *Swertia corymbosa*, Chem. Biodivers. 12 (3) (2015) 358–370, https://doi.org/10.1002/cbdv.201400055.
[43] H. Lineweaver, D. Burk, The determination of enzyme dissociation constants, JACS 56 (3) (1934) 658–666, https://doi.org/10.1021/ja01318a036.
[44] P. Masson, M.T. Froment, E. Gillon, F. Nachon, O. Lockridge, L.M. Schopfer, Kinetic analysis of effector modulation of butyrylcholinesterase-catalysed hydrolysis of acetanilides and homologous esters, FEBS J. 275 (10) (2008) 2617–2631, https://doi.org/10.1111/j.1742-4658.2008.06409.x.